Received: 25 April 2018 | Revised: 19 November 2018 | Accepted: 29 November 2018

DOI: 10.1002/asl.874

Atmospheric Science Letters RMetS

RESEARCH ARTICLE

The characteristics and classification of eastward-propagating mesoscale convective systems generated over the second-step terrain in the Yangtze River Valley

Ruyi Yang[1,2] | Yuanchun Zhang[1] | Jianhua Sun[1,2,3] | Shenming Fu[1,4] | Jun Li[5]

[1]Key Laboratory of Cloud–Precipitation Physics and Severe Storms (LACS), Institute of Atmospheric Physics, Chinese Academy of Sciences, Beijing, China

[2]University of the Chinese Academy of Sciences, Beijing, China

[3]Collaborative Innovation Center on Forecast and Evaluation of Meteorological Disasters, Nanjing University of Information Science and Technology, Nanjing, China

[4]International Center for Climate and Environment Sciences (ICCES), Institute of Atmospheric Physics, Chinese Academy of Sciences, Beijing, China

[5]31010 PLA Troops, Beijing, China

Correspondence
Yuanchun Zhang, Institute of Atmospheric Physics, Chinese Academy of Sciences, Beijing, China.
Email: zhyc@mail.iap.ac.cn

Funding information
National Natural Science Foundation of China, Grant/Award Number: 41505038, 91637211 and 41575045

A total of 316 eastward-propagating mesoscale convective systems (MCSs) that form over the second-step terrain are detected during May to August 2000–2016 (except 2005) using an hourly black body temperature (TBB) dataset. These MCSs last from three to dozens of hours and moved along various trajectories. These detected MCSs are divided into four categories (i.e., C1, C2, C3, and C4) according to their key characteristics. C1 MCSs generally move in a northeastward direction to northern China and have a mean duration of ~16 hr, while their C2 counterparts are mostly characterized by quasi-stationary behavior over the eastern edge of the second-step terrain and have a 9-hr mean life span approximately. In contrast, most C3 MCSs move in an eastward direction and tend to last ~21 hr on average, inducing heavy rainfall from the eastern edge of the second-step terrain to the coastline. The C4 MCSs possess similar features to C3 MCSs but have much shorter mean durations (~8 hr) and exert influences within an area mainly limited to the middle reaches of the Yangtze River Valley. Composite analyses of these four MCS categories show that a strong lower-level cyclonic vorticity in all categories favors the MCSs' sustainment; the differences of the steering flow from middle-to-upper levels account for the different moving directions of the four categories; the intensity of imported water vapor is proportional to the longevity of MCSs.

KEYWORDS

heavy rainfall, mesoscale convective systems, second-step terrain, Yangtze River Valley

1 | INTRODUCTION

Mesoscale convective systems (MCSs) are well-known for their significant role in generating hazardous weather conditions, such as heavy rain, lightning, and hail. Following Maddox (1980), numerous research studies have evaluated the statistical features of MCSs by defining size and duration criteria of the cold cloud shields based on infrared (IR) satellite images for various regions (Laing and Fritsch, 1997; Anderson and Arritt, 1998; Mathon and Laurent, 2001; Jirak *et al.,* 2003; Zheng *et al.,* 2008; Yang *et al.,* 2015). It is found that the formation of MCSs is typically associated with weak mid-tropospheric short-wave troughs and weak surface fronts, and their development is often supported by the low-level thermal forcing and convective instability.

In previous studies, Anderson and Arritt (1998) demonstrated that MCSs initiate in environments characterized by

deep, synoptic-scale ascent and in the presence of abundant low-level moisture transported by a southerly low-level jet (LLJ) associated with continental-scale baroclinic waves. The majority of MCSs inducing heavy rainfall within the Yangtze River valley (YRV) and Yangtze-Huai River valleys (YHRV) are associated with the Meiyu front, which encompasses the area between the second-step terrain (i.e., the Sichuan Basin and the Qinling and Wushan mountains) (Figure 1) and the middle reaches of the YRV and YHRV (Zhang *et al.,* 2004; Sun *et al.,* 2010; Meng *et al.*, 2013; Zheng *et al.,* 2013; Yang *et al.,* 2015). Although recent studies have demonstrated that MCSs generated over the second-step terrain could move eastward and influence precipitation in downstream regions (Sun and Zhang, 2012; Zhang and Sun, 2017), most of them were based on specific case studies, which could not feature the universal characteristics of this type of event. Therefore, it is useful to evaluate the statistical features of the eastward-propagating MCSs generated over the second-step terrain, to elucidate the ambient environments favorable for their evolution and propagation, and to explore their influences on downstream precipitation.

2 | DATA AND METHODS

The hourly black body temperature (TBB) IR1 records from Japanese satellites at 0.05° × 0.05° horizontal resolution (http://weather.is.kochi-u.ac.jp/archive-e.html) between May and August from 2000 to 2016 (except 2005) are utilized to detect MCSs over the study region (106°–113°E, 28°–35°N, the red box in Figure 1). Data for 2005 are not included for analysis because of the large missing rate in this year. The hourly precipitation observation from 2,420 surface stations provided by the Chinese Meteorological Administration (CMA) is used to study the precipitation associated with the MCSs. The 6-hr climate forecast system reanalysis (CFSR) data (0.5° × 0.5°) from the National Centers for Environment Prediction (NCEP) are utilized to composite the background circulation.

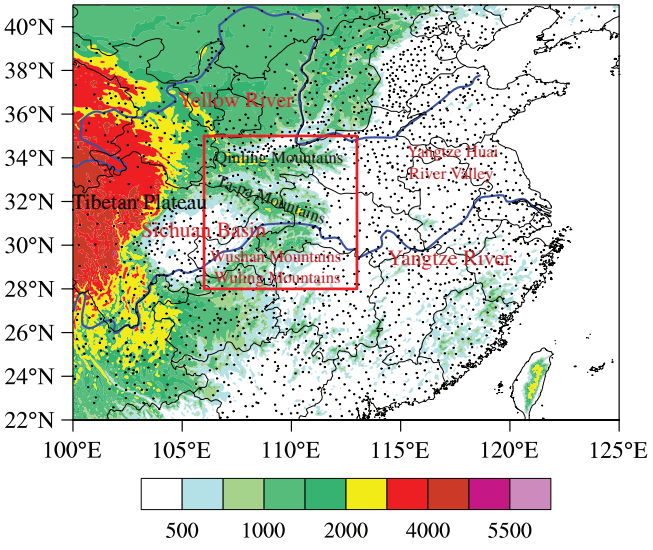

FIGURE 1 Geographic distribution of elevations in East China (shading, units: m). The red box denotes the MCS formation study area. The black dots are stations with hourly precipitation observation

The definition of an eastward-propagating MCS over the second-step terrain in this study is defined based on previous studies (Maddox, 1980; 1983; Augustine and Howard, 1988; 1991; Cotton *et al*., 1989; Mathon *et al*., 2002; Zheng *et al.,* 2008; Zhuo *et al.,* 2012). First, at the time of initiation, the MCS's center should be located within the study region. The detecting criteria are as follows:

1. The MCS's contiguous cloud shield (TBB ≤ −52°C) should be no less than 5,000 km^2 (i.e., ≥5,000 km^2)
2. The duration of the MCS should be no shorter than 3 hr (i.e., ≥3 hr)
3. After initiation, there is at least one instance for which the location of the MCS's center is located east of its formation location and has a corresponding terrain height less than 500 m
4. The MCS is no longer tracked and considered terminated when its size as defined in condition 1 falls below 5,000 km^2. Based on the above criteria, the detection and tracking of MCSs are first implemented via an automated objective method (Li *et al.,* 2012a, 2012b; Li *et al.,* 2015), and then, a manual validation is used to improve the results.

Three typical stages of an MCS are investigated in detail. This includes the initiation, maturity, and termination. The initiation is defined as the first time that an MCS satisfies Criterion 1; the maturation is defined as the time when the cloud shield area of an MCS reaches its maximum; and the termination is defined as the first time that an MCS no longer satisfies Criterion 1. Additionally, taking into account the MCS initiation and termination locations, as well as trajectories, propagating speed, directions, and durations, a series of curve-aligned clustering algorithms based on polynomial regression mixture models (Gaffney, 2004) are implemented to classify the tracks of these eastward-propagating systems.

3 | RESULTS

3.1 | Basic statistical features of MCSs

A total of 316 eastward-propagating MCSs are identified. The inter-annual frequency of these systems varies considerably from 11 (minimum) in 2012 and 2014 to 36 (maximum) in 2007, with an annual mean frequency of ~20 (Figure 2a). The MCS occurrences increase monthly between May and July, while decrease in August (Figure 2b). Their maximum MCS occurrence is found in July, accounting for ~50% of

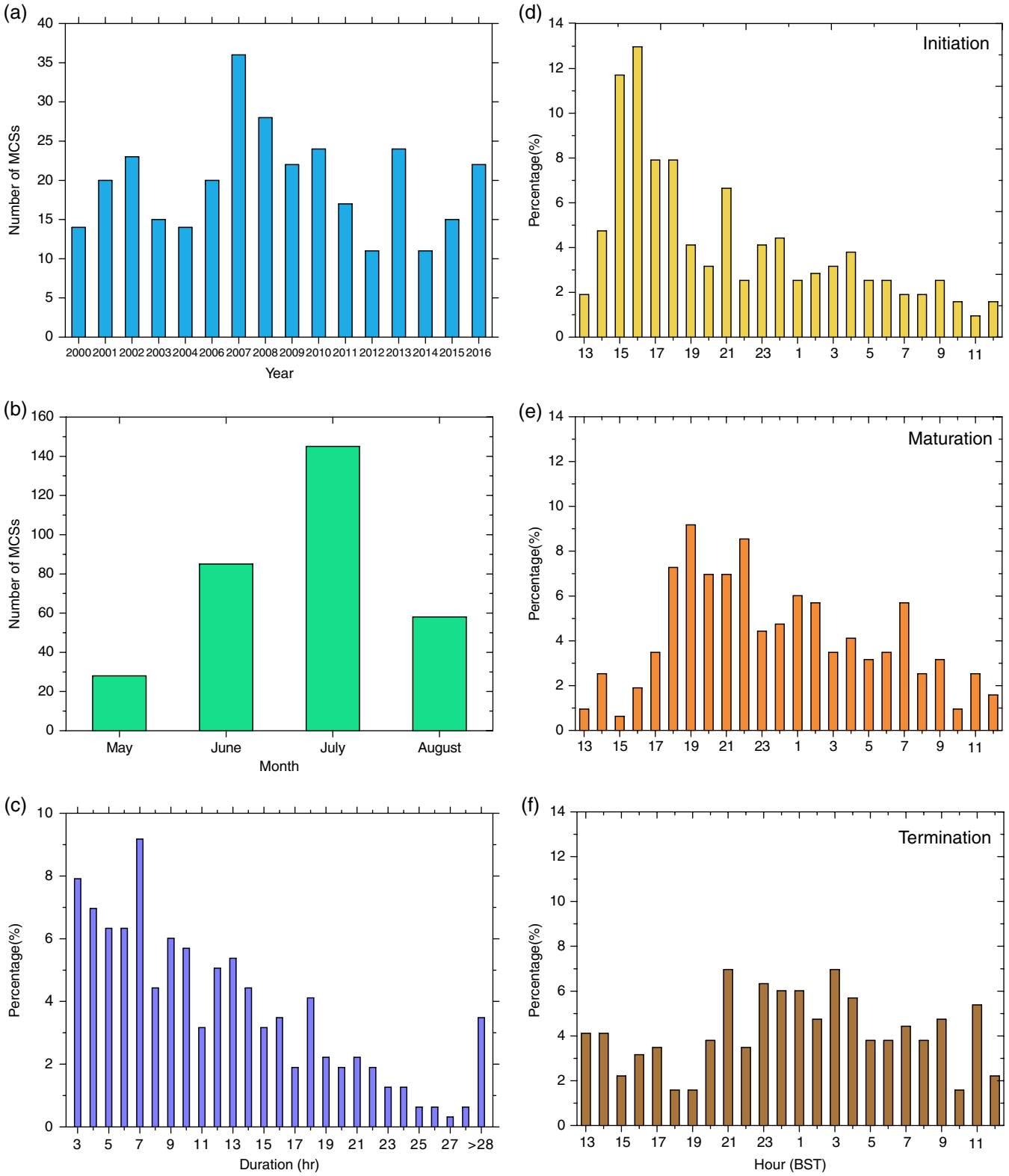

FIGURE 2 The annual variations (a), monthly variations (b) and duration (c) of the eastward-propagation MCSs; (d–f) are the diurnal variations of the MCSs initiation, maturation and termination, respectively

the total numbers (Figure 2b), which is consistent with Yang *et al*. (2015).

Figure 2d illustrates that the peak of the initiation of the eastward-propagating MCSs appears in the afternoon and early evening (1500–1800 BST), which is consistent with records from other regions (Laing and Fritsch, 1997; Machado *et al.,* 1998; Pope *et al.,* 2008; Yang *et al.,* 2015). Typically, the eastward-propagating MCSs reach the maximum extent in the evening (1800–2200 BST, Figure 2e) before their subsequent termination (ca. 2300 BST, Figure 2f). The termination of MCSs vary slightly from the evening to the next morning (2300–0400 BST, Figure 2f).

The termination locations of the eastward-propagating MCSs encompass a large region that span from the middle reaches of the YRV to the oceans. The MCS durations range from a minimum of 3 hr (i.e., the lowest time limit for objective tracking) to over 20 hr. Overall, as the MCSs' duration increase, their corresponding frequency of occurrence decrease, and its peak appears at 7 hr.

Figure 3a summarizes the total trajectories of eastward-propagating MCSs. Most MCSs are initiated on the eastern edge of the second-step terrain (denoted by red dots in Figure 3a) and some initially appear in the high mountains and a few begin over the Sichuan Basin. The majority of MCSs move in an eastward direction during their evolution; some reach only as far as the middle reaches of the YRV (~116°E), while some arrive at the YHRV (~120°E), and others even influence the oceanic areas. Some of the tracked MCSs move northeastward to northern China and onto the Korean Peninsula, while a small number terminate in southeastern regions of the study area (denoted by the purple dashed box in Figure 3) and on the Yunnan-Kweichow Plateau.

Depending on their trajectories (Figure 3a), the evolution of MCSs and their impact on regional rainfall vary from the second-step terrain to the lower downstream reaches. Four track categories are clustered (Figure 3b–e, Gaffney, 2004), including Category 1 (C1; Figure 3b) that comprised a set of 42 MCSs that move northeastward and that have an average duration of 16 hr (Figure 3b). In contrast, most C2 MCSs (including 102 cases) remain quasi-stationary and have a mean lifetime of 9 hr (Figure 3c). The MCSs classified as C3 (i.e., a set of 55 MCSs; Figure 3d) tend to move in an eastward direction and last for about 22 hr on average; some of these even move into the eastern oceans (Figure 3d). All the remaining 117 MCSs are classified as C4. These systems also tend to move eastward and have an average life span of 8 hr. Most of these MCSs influence precipitation over the middle reaches of the YRV (Figure 3e).

The bulk of the four eastward-propagating MCS categories is found over the eastern edge of the second-step terrain and extend into the middle reaches of the YRV, except for the C1 group. The different trajectories of the four categories are related to steering winds at the middle and upper levels, and large-scale conditions at lower levels influence the initiation and development of convection. The comparisons of the large-scale circulations among the four categories will be discussed in the next section.

3.2 | Comparisons of large-scale circulations

The composite lifetime circulations are different at both upper and lower levels within the four MCS categories (Figure 4); in the case of C1 MCSs, South Asian High at 200 hPa controls low to middle latitude regions while a weak trough maintains over the Sichuan Basin. An upper-level jet (ULJ, wind speed greater than 25 m/s) is separated into the western and eastern parts (Figure 4a). The divergence appears on the right side of the entrance region of the eastern part ULJ, the formation and enhancement of convection is perpendicular to the ULJ (Figure 4a). Similar to the circulation at 200 hPa, a trough at the middle level (500 hPa) is also present in this case that extends from the Sichuan Basin to the second-step terrain, while western pacific subtropical high (WPSH) covers both South China and YHRV. Combined with western steering flow (Figure 4b), the MCSs propagate northeastward, while a lower level southerly wind (850 hPa) transports abundant water vapor into the study area alongside a convergent belt that extends from the eastern edge of the second-step terrain into northern China (~35°N, Figure 4c). Strong positive vorticity is consistent with the regions of MCSs' formation (Figure 4c).

The composite circulation of C2 MCSs at 200 hPa is different from their C1 counterparts (Figure 4d). The entire study region is controlled by the South Asian High while the ULJ dominates regions to the west of 125°E. The strong isobaric gradient corresponds with the ULJ belt. At the middle level (Figure 4e), WPSH extends west of 105°E and a westerly wind covers the areas east of the second-step terrain. Southwestern wind at 850 hPa promotes the convergence of water vapor within the southeastern area of the study region (Figure 4f), while large-scale circulations at middle and lower levels remain favorable for the formation and maintenance of C2 MCSs over the eastern edge of the second-step terrain.

The ULJ of C3 MCSs at 200 hPa (Figure 4g) is stronger than the cases for C2, meaning that the more intense divergence over the study region promotes the formation of stronger and more convection systems; at the middle level (500 hPa, Figure 4h), the WPSH extends westward to ~95°E and a weak low trough is located to the east of the Tibetan Plateau, similar to the situation for C2 MCSs. However, the steering effect in the middle and upper levels favors the MCSs propagating eastward; a stronger southwesterly wind at 850 hPa transports more water vapor from eastern low-lying regions downstream of the second-step terrain into the oceanic region (Figure 4i). Upper- and mid-level circulations of C4 MCSs are similar to those of C1 MCSs and the presence of a low trough to the east of the Tibetan Plateau steers these systems to the east (Figure 4k). However, consistent with southwestern wind water vapor transportation over the mainland east of the second-step terrain (Figure 4l), C4 MCSs mostly terminate over the middle-to-lower reaches of the YRV.

Composite circulations of the four MCS categories reveal that strong positive vorticity maxima at lower levels are consistent with MCSs formation locations. Southwesterly or westerly winds at upper and middle levels act to steer the displacement and propagation of the

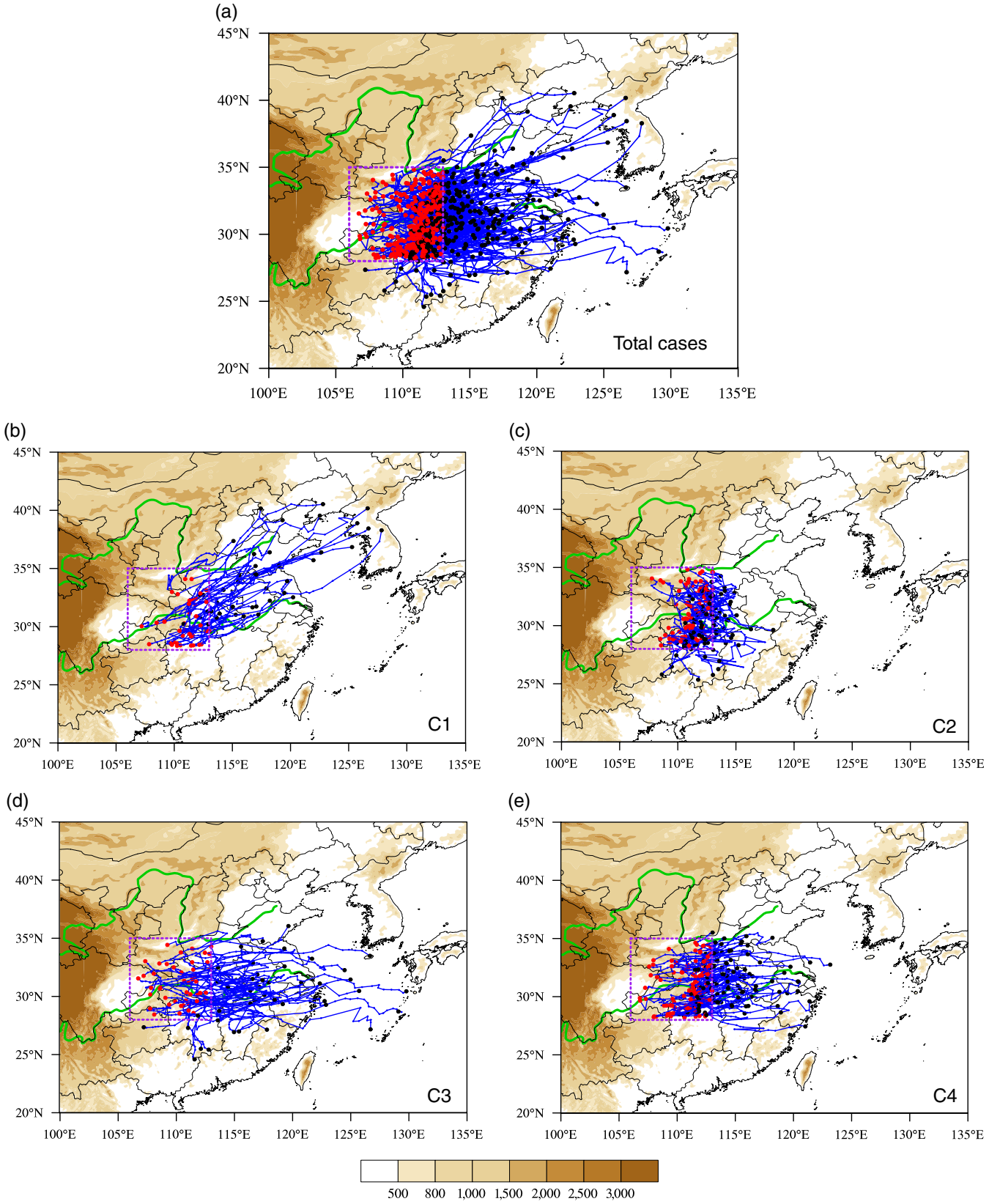

FIGURE 3 Tracks of eastward-propagating MCSs of (a) the overall total, (b) C1, (c) C2, (d) C3, and (e) C4. The red dots on these maps denote MCSs formation locations, while the black dots denote termination locations. The blue lines mark trajectories from initiation to termination, while the purple dashed boxes denote MCS formation regions. Colored shading denotes elevations higher than 500 m

MCSs, while the intensity of water vapor flux transported by the southwesterly winds influences the durations of these systems.

3.3 | MCS associated precipitation

From the frequency distribution of the eastward-propagating MCSs and the percentages of MCS-related precipitation to

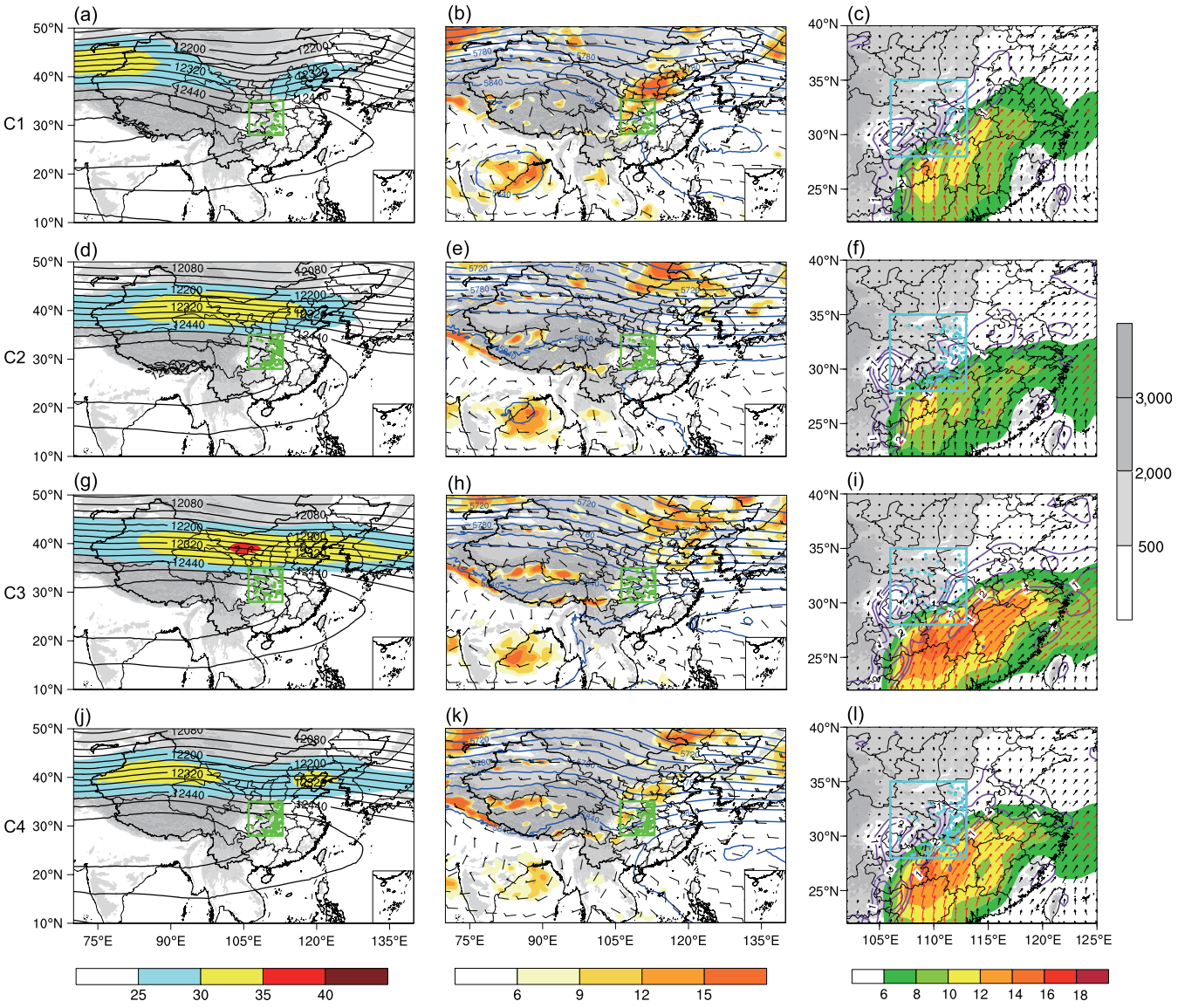

FIGURE 4 Composite background circulations for the four MCS categories from upper to lower levels. In the case of C1, (a) geopotential height (black line, unit: gpm) and wind speeds larger than 25 m/s(color shading, unit: m/s) at 200 hPa, while (b) geopotential height (blue line, unit: gpm) and relative vorticity (shading, unit: 10^{-6} s^{-1}) at 500 hPa, and (c) relative vorticity (purple line, unit: 10^{-5} s^{-1}), wind field (black vectors, unit: m/s, wind speeds greater than 6 m/s are denoted by red vectors), and the value of water vapor flux (color shading, unit: g·s·kg^{-1}) at 850 hPa. The maps in (d), (e), and (f) are the same as in (a), (b), and (c) but for C2, while those in (g), (h), and (i) are for C3, and those in (j), (k), and (l) stand for C4. Dots mark MCS formation locations, while inner boxes denote formation regions, and gray shading indicates elevations higher than 500 m

total warm-season precipitation (Figure 5), it can be seen that the maximum rainfall frequency is over the eastern edge of the second-step terrain as well as in the middle reaches of the YRV and the precipitation related to eastward-propagating MCSs accounts for more than 35% of the total warm-season precipitation. In Section 3.2, it is shown that the four categories of eastward-propagating MCSs could influence the precipitation in different downstream regions. In addition, four precipitation intensity levels are defined in the precipitation analysis: light (between 0.1 and 2.5 mm/hr), moderate (between 2.6 and 8.0 mm/hr), heavy (between 8.1 and 15.9 mm/hr), and torrential (>16 mm/hr). The accumulated MCS-related rainfall and contribution of MCS-related precipitation of different intensity levels to the corresponding warm-season total precipitation are compared among the four categories in Figure 5. It is clearly shown that the total MCS-related rainfall increases from light to torrential intensity level and has a significant impact on downstream areas, especially over the middle reaches of the YRV. For the four categories (Figure 5), the increased percentage from light to torrential hourly precipitation demonstrates that the eastward-propagating MCSs often tend to induce precipitation that is stronger than moderate rainfall, and the accumulated precipitation and percentages maxima appear in the middle of YRV. Compared with other three categories, the C3 MCSs cause the heaviest precipitation, which extends from the eastern edge of the second step terrain to the eastern coast lines. In addition, the percentage of C3 MCS-related

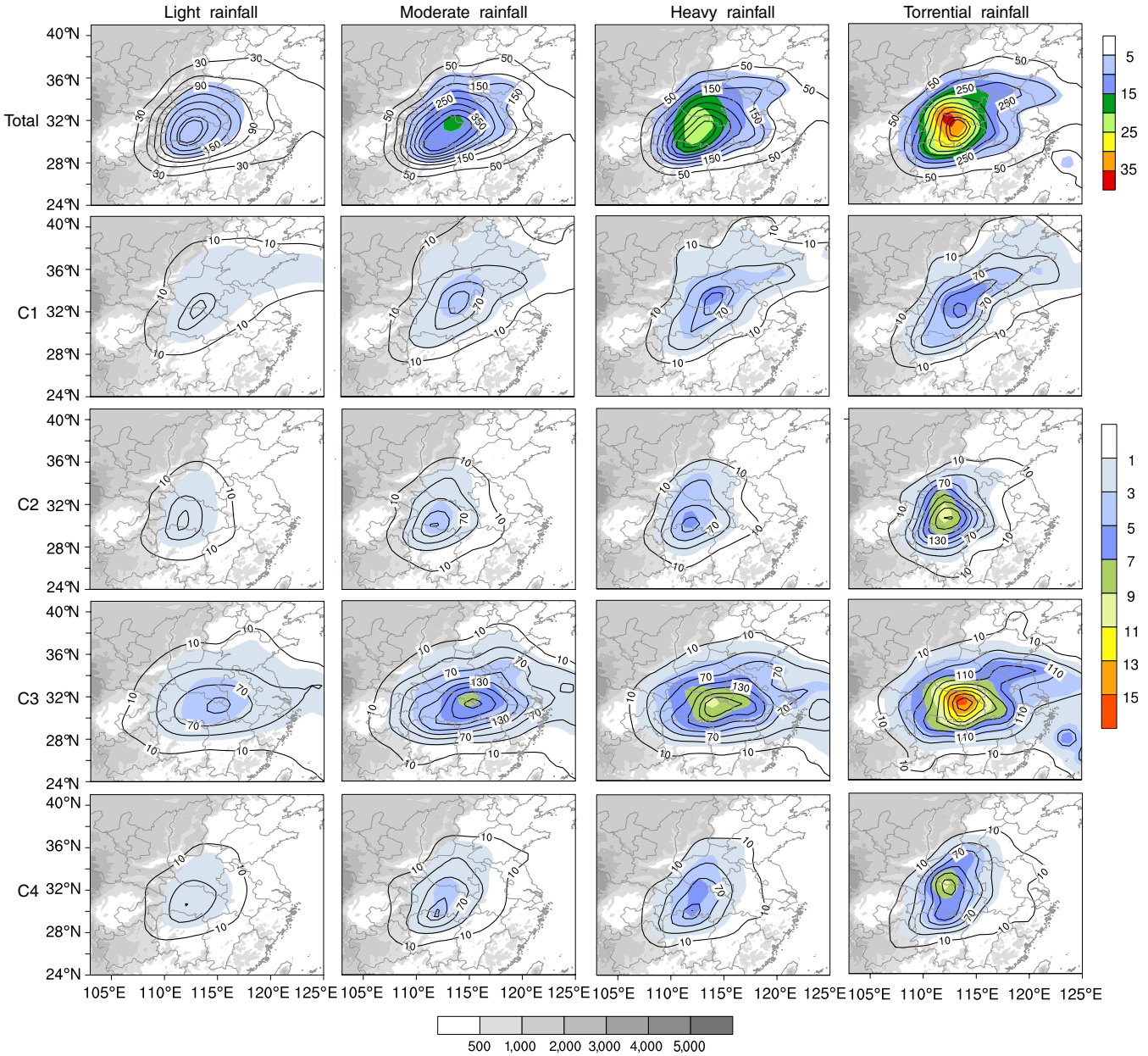

FIGURE 5 Accumulated precipitation (black line, unit: mm) and the percentages (color shading, unit: %) of MCS-related precipitation to totals between May and August for different precipitation intensity level: (top) all MCS and (bottom) the four MCS categories (C1-C4). The gray shading denotes elevations higher than 500 m

precipitation to totals between May and August is the highest regardless of the precipitation intensity levels. The rainbelt of C1 MCSs covers from the middle of YRV to North China in northeastern-southwestern direction. The C2 and C4 MCSs mainly influence the rainfall in the middle of YRV. Additionally, compared with other three categories, the C4 MCSs-related light rainfall contributes the least to the total rainfall. For the moderate and heavy rainfall, the accumulated rainfall and percentages of C1, C2 and C4 MCSs-related precipitation are similar, however, the percentage of C1 MCSs-related torrential rainfall to the total warm-season corresponding rainfall level is lowest among the four categories.

4 | CONCLUSIONS AND DISCUSSIONS

A total of 316 eastward-propagating MCSs are identified over the second-step terrain in 16 summers using hourly TBB data from Japanese satellites. These important weather systems frequently induce heavy rainfall in downstream regions east of the second-step terrain, and considerable inter-annual variability in their occurrence frequency is also observed, at a mean of ~20. The monthly number of MCSs reaches a maximum in July, while the duration lasted from 3 hr to more than 20 hr. Most of the eastward-propagating MCSs initiate along the eastern edge of the second-step terrain and peak between the afternoon and early evening; these systems mostly mature

about 4 hr after initiation when they move into the middle reaches of the YRV. Their terminations mainly occur subsequent to the late evening in locations ranging from the middle reaches of the YRV to the eastern oceans.

Four categories of MCSs are classified using a curve-aligned clustering model approach. C1 MCSs mostly move to the northeast into northern China and influence precipitation from the eastern edge of the second-step terrain to Shandong Province. Due to the combined influence of weaker westerly and southwesterly winds at 500 and 850 hPa, respectively, C2 MCSs generally remain quasi-stationary over the eastern edge of the second-step terrain and the middle reaches of YRV, inducing heavy rainfall over these regions. C3 MCSs make the largest contribution to seasonal heavy rainfall among the four categories as a stronger mid-level westerly wind combined with abundant water vapor at lower levels from the mainland to the oceans favors their eastward movement and longevity. Finally, C4 MCSs mainly influence regional precipitation from the eastern edge of the second-step terrain to the middle reaches of the YRV.

This statistical study points out that the eastward-propagating MCSs can frequently occur over the second-step terrain, and these MCSs contribute considerably to the seasonal heavy rainfall over the middle and lower reaches of the YR. In addition, through compositing, favorable large-scale circulations for the MCSs' formation (that originate over the second step terrain), propagation and sustainment are established and compared with each other. These results could be helpful for understanding precipitation over the YR, and to improve the precipitation forecast in the downstream regions of the second-step terrain. Moreover, it can also be regarded as the basis for further mechanism research of these MCSs evolution.

ACKNOWLEDGEMENT

This research was supported by the National Natural Science Foundation of China (Grants Nos. 41505038, 91637211 and 41575045).

ORCID

Yuanchun Zhang https://orcid.org/0000-0003-3038-9320
Shenming Fu https://orcid.org/0000-0001-9670-0607

REFERENCES

Anderson, C.J. and Arritt, R.W. (1998) Mesoscale convective complexes and persistent elongated convective systems over the United States during 1992 and 1993. *Monthly Weather Review*, 126, 578–599.

Augustine, J.A. and Howard, K.W. (1988) Mesoscale convective complexes over the United States during 1985. *Monthly Weather Review*, 116, 685–701.

Augustine, J.A. and Howard, K.W. (1991) Mesoscale convective complexes over the United States during 1986 and 1987. *Monthly Weather Review*, 119, 1575–1589.

Cotton, W.R., Lin, M.S., McAnelly, R.L. and Tremback, C.J. (1989) A composite model of mesoscale convective complexes. *Monthly Weather Review*, 117, 765–783.

Gaffney, S.J. (2004) *Probabilistic curve-aligned clustering and prediction with regression mixture models*. Irvine, CA: University of California, pp. 1–281.

Jirak, I.L., Cotton, W.R. and McAnelly, R.L. (2003) Satellite and radar survey of mesoscale convective system development. *Monthly Weather Review*, 131, 2428–2449.

Laing, A.G. and Fritsch, J.M. (1997) The global population of mesoscale convective complexes. *Quarterly Journal of the Royal Meteorological Society*, 123, 389–405.

Li, J., Wang, D.H. and Wang, B. (2012a) Structure characteristics of moist neutral stratification in a mesoscale convective system. *Climatic and Environmental Research*, 17, 617–627 (in Chinese).

Li, J., Wang, B. and Wang, D.H. (2012b) The characteristics of mesoscale convective systems (MCSs) over East Asia in warm seasons. *Atmospheric and Oceanic Science Letters*, 5, 102–107.

Li, J.Y., Shen, X.Y., Wang, D.H. and Li, J. (2015) Distribution and characteristic of the MCS over South China during the spring and summer of 2008. *Journal of Tropical Meteorology*, 31, 475–485 (in Chinese).

Machado, L., Rossow, W., Geudes, R. and Walker, A. (1998) Life cycle variations of mesoscale convective systems over the America. *Monthly Weather Review*, 126, 1630–1654.

Maddox, R.A. (1980) Mesoscale convective complexes. *Bulletin of the American Meteorological Society*, 61, 1374–1387.

Maddox, R.A. (1983) Large-scale meteorological conditions associated with midlatitude, mesoscale convective complexes. *Monthly Weather Review*, 111, 1475–1493.

Mathon, V. and Laurent, H. (2001) Life cycle of Sahelian mesoscale convective cloud systems. *Quarterly Journal of the Royal Meteorological Society*, 127, 377–406.

Mathon, V., Laurent, H. and Lebel, T. (2002) Mesoscale convective system rainfall in the Sahel. *Journal of applied meteorology*, 41, 1081–1092.

Meng, Z.Y., Yan, D.C. and Zhang, Y.J. (2013) General features of squall lines in East China. *Monthly Weather Review*, 141, 1629–1647.

Pope, M., Jakob, C. and Reeder, M.J. (2008) Convective systems of the north Australian monsoon. *Journal of Climate*, 21, 5091–5112.

Sun, J.H. and Zhang, F.Q. (2012) Impacts of mountain-plains solenoid on diurnal variations of rainfalls along the Mei-yu front over the East China plains. *Monthly Weather Review*, 140, 379–397.

Sun, J.H., Zhao, S.X., Xu, G.K. and Meng, Q.T. (2010) Study on a mesoscale convective vortex causing heavy rainfall during the Mei-yu season in 2003. *Advances in Atmospheric Sciences*, 27, 1193–1209.

Yang, X., Fei, J., Huang, X., Cheng, X., Carvalho, L.M. and He, H. (2015) Characteristics of mesoscale convective systems over China and its vicinity using geostationary satellite FY2. *Journal of Climate*, 28, 4890–4907.

Zhang, Y.C. and Sun, J.H. (2017) Comparison of the diurnal variations of precipitation east of the Tibetan Plateau among sub-periods of Meiyu season. *Meteorology and Atmospheric Physics*, 129, 539–554.

Zhang, X.L., Tao, S.Y. and Zhang, S.L. (2004) Three types of heavy rainstorms associated with the Mei-yu front. *Chinese Journal of Atmospheric Sciences*, 28, 187–205 (in Chinese).

Zheng, Y.G., Chen, J. and Zhu, P.J. (2008) Climatological distribution and diurnal variation of mesoscale convective systems over China and its vicinity during summer. *Chinese Science Bulletin*, 53, 1574–1586.

Zheng, L.L., Sun, J.H., Zhang, X.L. and Liu, C.H. (2013) Organizational modes of mesoscale convective systems over central East China. *Weather Forecasting*, 28, 1081–1098.

Zhuo, H., Zhao, P., Li, C.H. and Pu, Z.X. (2012) Analysis of climatic characteristics of mesoscale convective system over the lower reaches of the Yellow River during summer. *Chinese Journal of Atmospheric Sciences*, 36, 1112–1122 (in Chinese).

How to cite this article: Yang R, Zhang Y, Sun J, Fu S, Li J. The characteristics and classification of eastward-propagating mesoscale convective systems generated over the second-step terrain in the Yangtze River Valley. *Atmos Sci Lett*. 2018;e874. https://doi.org/10.1002/asl.874